Skeletal Radiology (2019) 48:791–802
https://doi.org/10.1007/s00256-018-2979-4

TECHNICAL REPORT

A prototype assembled 3D-printed phantom of the glenohumeral joint for fluoroscopic-guided shoulder arthrography

Ramin Javan[1] · **Amy L. Ellenbogen**[1] · **Nicholas Greek**[2] · **Shawn Haji-Momenian**[1]

Received: 11 February 2018 / Revised: 7 May 2018 / Accepted: 14 May 2018 / Published online: 9 June 2018

Abstract

Purpose To describe the methodology of constructing a three-dimensional (3D) printed model of the glenohumeral joint, to serve as an interventional phantom for fluoroscopy-guided shoulder arthrography training.

Materials and methods The osseous structures, intra-articular space and skin surface of the shoulder were digitally extracted as separate 3D meshes from a normal CT arthrogram of the shoulder, using commercially available software. The osseous structures were 3D-printed in gypsum, a fluoroscopically radiopaque mineral, using binder jet technology. The joint capsule was 3D printed with rubber-like TangoPlus material, using PolyJet technology. The capsule was secured to the humeral head and glenoid to create a sealed intra-articular space. A polyamide mold of the skin was printed using selective laser sintering. The joint was stabilized inside the mold, and the surrounding soft tissues were cast in silicone of varying densities. Fluoroscopically-guided shoulder arthrography was performed using anterior, posterior, and rotator interval approaches. CT arthrographic imaging of the phantom was also performed.

Results A life-size phantom of the glenohumeral joint was constructed. The radiopaque osseous structures replicated in-vivo osseous corticomedullary differentiation, with dense cortical bone and less dense medullary cancellous bone. The glenoid labrum was successfully integrated into the printed capsule, and visualized on CT arthrography. The phantom was repeatedly used to perform shoulder arthrography using all three conventional approaches, and simulated the in vivo challenges of needle guidance.

Conclusions 3D printing of a complex capsule, such as the glenohumeral joint, is possible with this technique. Such a model can serve as a valuable training tool.

Introduction

Shoulder arthrography is typically performed to evaluate the rotator cuff and/or labrum [1, 2]. Although 3-Tesla MR imaging has decreased the utilization of MR arthrography (MRA), studies have shown additional diagnostic benefits of MRA [3], particularly in the setting of partial-thickness rotator cuff tears, labral tears, and previous cuff or labral surgery [4]. Fluoroscopy-guided shoulder arthrography remains an important skill for radiologists. Conventional needle access into the joint includes anterior [5], posterior [6], and rotator interval [7] approaches. With experience, the joint can be accessed quickly and easily, minimizing patient discomfort, fluoroscopy time (radiation exposure), and extra-articular injection of contrast medium (which can simulate pathological conditions on CT/MR arthrography).

Currently, most trainees learn these procedures by “seeing one” and then “doing one” on patients for the first time, under attending supervision. With advancements in 3D printing technology, printed models are becoming powerful medical tools for trainee teaching, and for patient education and surgical planning [8, 9]. 3D printed models have been used to render complex hepatic [10], osseous [11], cardiovascular [12], prostatic, and vascular anatomy [13]. 3D printed phantoms have also been used to teach procedural skills, including placement of external ventricular drains [14], femoral central line access [15], facet joint injection [16], lumbar puncture [17], and epidural and nerve root injections [18].

The 3D printing of a glenohumeral joint phantom poses several new challenges, including:

✉ Ramin Javan
rjavan@mfa.gwu.edu

Amy L. Ellenbogen
ale2t@virginia.edu

Nicholas Greek
msdnhg@email.gwu.edu

Shawn Haji-Momenian
shawnhm@gmail.com

[1] Department of Radiology, George Washington University Hospital, 900 23rd St NW, Suite G2092, Washington, DC 20037, USA

[2] Clinical Learning and Simulation Skills (CLASS) Center, George Washington University School of Medicine, 2300 I (Eye) Street, NW, Ross Hall 405, Washington, DC, USA

1. Creation of a complex-shaped "soft" needle-penetrable sealed joint capsule
2. Incorporation of the glenoid labrum into the intra-articular anatomy
3. Utilization of multi-substance 3D printed components to construct a phantom with radiopaque bones and lucent life-like soft tissues for use under fluoroscopy

Basics steps in 3D printing begin with the "segmentation" of image data [19]. Segmentation is the extraction of a subset of pertinent image data as two-dimensional (2D) layers or "masks," which are compiled to create a 3D "mesh." Segmentation is the most important step in creating the digital object that is to be printed. Mesh data can then be used to print the object in a variety of substances using different printing technologies [20, 21].

The purpose of this study was to construct a 3D-printed, anatomically accurate life-size phantom of the shoulder, to simulate fluoroscopy-guided shoulder arthrography for all three conventional approaches. Multiple printing technologies, including binder jet, Polyjet, and selective laser sintering were used. A novel application of gypsum binder jet printing is described for the first time, allowing for printing of osseous structures with corticomedullary differentiation. An innovative subtraction technique is also described for creating the complex glenohumeral joint capsule. To the best of our knowledge, this is the first paper describing the construction of a 3D-printed glenohumeral joint phantom for these purposes, where trainees can repeatedly practice the procedure before ever seeing their first patient.

Materials and methods

Segmentation of the shoulder

The shoulder joint was digitally segmented as three separate components: osseous structures, intra-articular space, and skin surface. The DICOM image data of a de-identified normal CT arthrogram (CTA) of the shoulder, acquired in slices 0.6-mm thick in a soft-tissue kernel, was imported into Materialise inPrint 2.0 (Leuven, Belgium), commercially available medical 3D printing software. This software was used to segment the osseous structures and contrast medium-filled intra-articular space using a "thresholding" technique. Thresholding sets the range of CT Hounsfield units (HU) to be segmented from the image data. A threshold minimum of 226 HU and maximum of 2,160 HU were used to segment the humerus, scapula, and clavicle as one osseous mask. A threshold minimum of 200 HU and maximum of 2,160 HU were used to segment the intra-articular space (as opacified by contrast medium) as a separate mask.

Because of an overlap in Hounsfield attenuation between contrast medium in the joint and cortical bone, the software's "Split" function was also used to assist in separating these structures as separate masks. Regions of interest (ROIs) were placed separately on bone or contrast; the software identifies contiguous pixels with similar attenuation as the same structure and assists in separating structures of similar density. Although threshold and split function segmentation of the osseous structures as a mask was relatively straightforward, segmentation of the contrast-filled intra-articular space required significant manual editing ("Brush" tool) to demarcate the capsule margins in all three planes. This had to be performed because thresholding and "split" function tools resulted in areas of irregular capsular surfaces, as attenuation shifts from bright contrast to soft-tissue attenuation over a few pixels at the capsule-soft tissue margins. This was a critical step in the development of this phantom. The final 2D masks of the bones and intra-articular space were reconstructed into the final 3D meshes (Fig. 1).

As explained in the discussions, the capsule had to be designed as a hollow socket-like structure, with the bony glenoid docking into the encapsulated base, and the humeral head telescoping into a hollow socket. To create the final mesh of the joint capsule, a "subtraction" technique was used. A 3D cube "bounding box," or ROI, was created (in Materialise inPrint) to encompass the entire joint; this was filled solid by setting minimum and maximum threshold values of 0 and 2160 respectively. The 3D reconstructions of the segmentation masks of the humeral head, glenoid, and the contrast medium-filled intra-articular space were then subtracted from the cube, leaving a hollow cavity. The resulting 3D mesh was then manually trimmed on the outside edges using the "Brush" tool in "Erase" mode, to create a joint capsule that was durable yet thin on its anterior and posterior margins to allow seamless needle entry (Fig. 2). Particular attention was given to capsular attachment sites on the greater and lesser tuberosities. The filling defects created by the labrum and bicipitolabral complex along the intra-articular space were included as part of the glenoid capsular margins. The remainder of the intra-articular segment of the long head of the biceps tendon was digitally erased. The capsule sites for arthrography needle access, along the anterior, posterior, and rotator interval margins of the segmentation mask were created with a thickness of 2 to 3 mm, to allow for easy passage of the needle into the joint. The remaining portions of the capsule had a thickness of 5 to 7 mm for greater strength. The communication of the intra-articular space with the long head of the biceps tendon sheath and bicipital groove was eliminated to simplify the capsular attachments. Last, the unnecessary bulky edges of the cube were digitally removed, saving printing material and reducing cost.

Although 3D meshes of the bones and capsule were created for direct printing, a mesh of the skin surface was made for creation of a mold for casting of the surrounding soft tissues. Freeware software OsiriX Lite's (Bernex, Switzerland) "surface rendering" tool (with predefined "skin" settings) was used to create a mesh of the skin surface from the CT arthrogram DICOM data (Fig. 3a). The mesh was exported as a stereolithography file (STL), a common 3D printing file format. This was first imported into Materialise inPrint to eliminate the

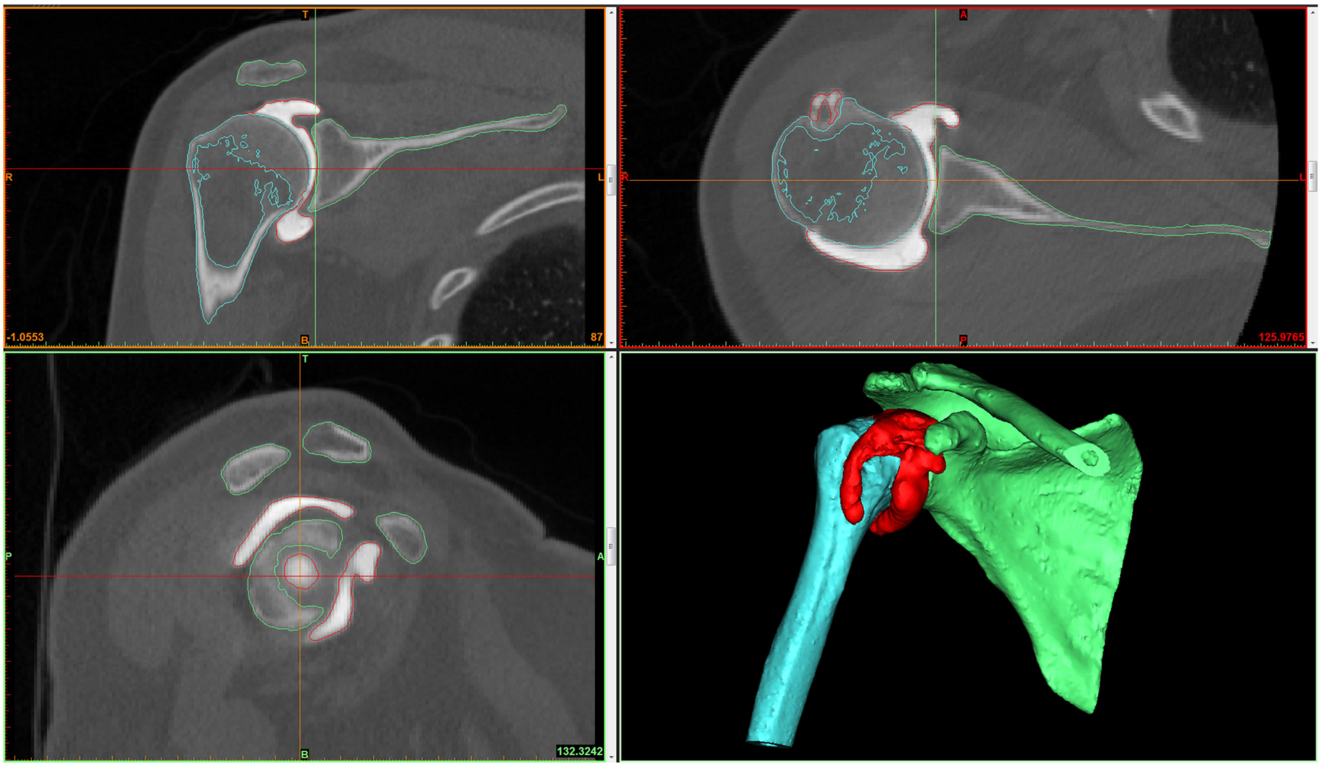

Fig. 1 Segmentation masks of the osseous structures and joint capsule (as defined by the contrast medium-opacified intra-articular space) created from a normal CT arthrogram in Materialise inPrint. Note that the contour deformity of the labrum is included as part of the capsular margin and becomes incorporated into the capsule. The planar masks are reconstructed into a 3D mesh (*bottom right*)

extra image data around the skin mold (CT table, sheets on the scanner table, etc.) using the “Lasso” tool in the 3D view panel. Furthermore, using the “Hollow Inside” tool, an arbitrary inward thickness of 5 mm was given to the skin mold. The skin surface, bones, and capsule meshes were then imported into Autodesk 3D Studio Max (San Rafael, CA, USA), a 3D graphic design software program, available as freeware for educators and students. The skin mesh was edited to have a flat inferior surface and a curved medial wall; an orifice was created in the superior surface at the neck to serve as a spout for the cast (Fig. 3b, c). The osseous structures were digitally fitted into the skin mesh, requiring the cropping of the medial segment of the clavicle. A small additional support strut was created to connect the clavicle to the scapula, as the clavicle and acromion were unattached. The humeral diaphysis was stabilized on the inferior surface of the mold, the medial border of the scapula abutted the curved medial

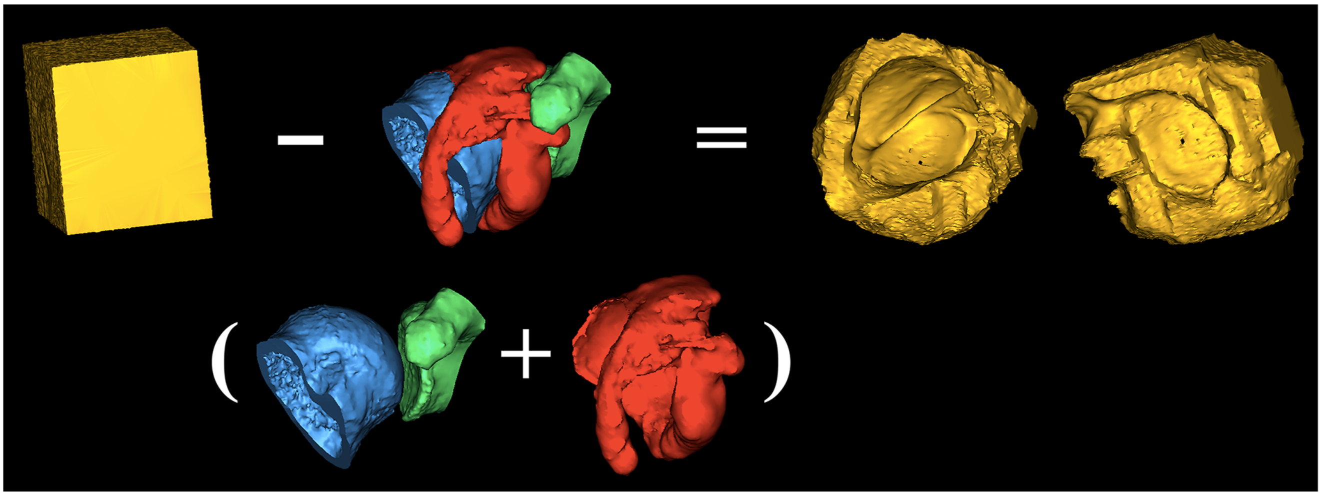

Fig. 2 The “subtraction” technique for creation of the joint capsule mesh. The 3D mesh of the humeral head, glenoid, and intra-articular space is subtracted from a solid bounding box, leaving a shell that was trimmed along the outside edges to create the final capsule mesh (shown from the medial and lateral sides)

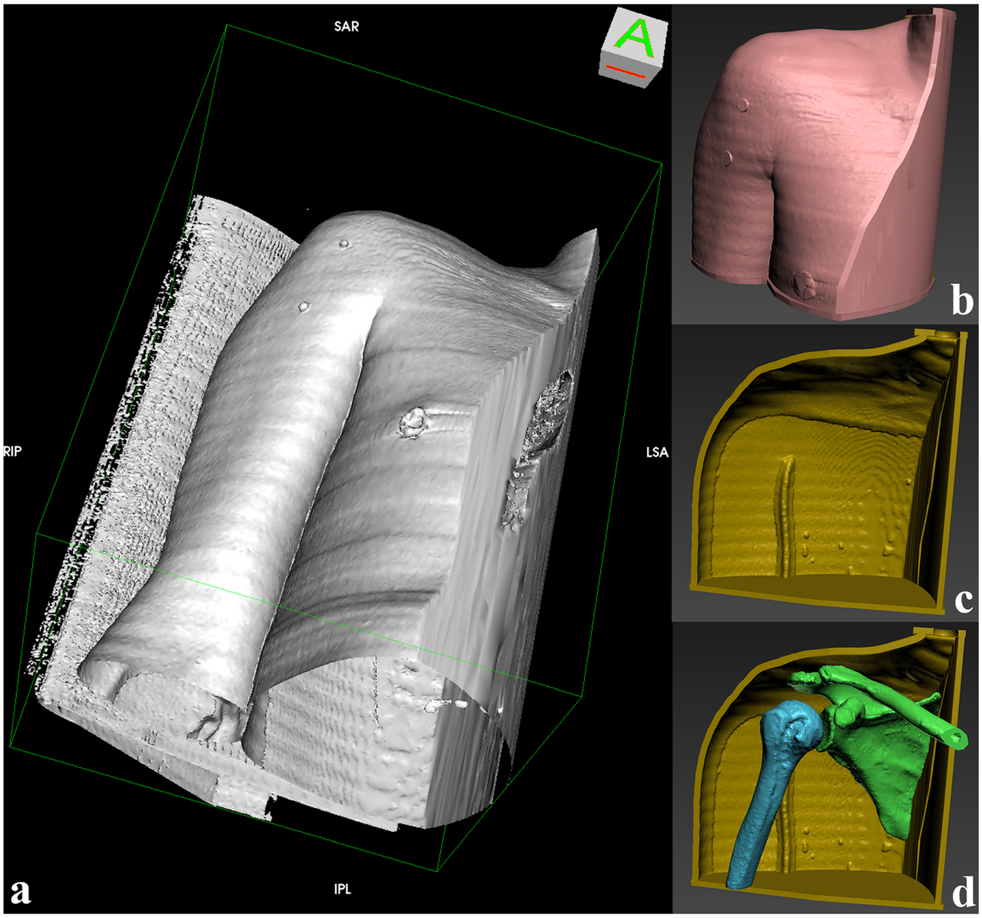

Fig. 3 Creation of the skin mold. **a** OsiriX Lite surface rendering of the skin using predefined values within the software. **b**–**d** Autodesk 3D Studio Max view of the finalized anterior and posterior halves of the skin mold, with fitting of the osseous structures inside the mold

wall of the mold, and the posterior surface of the scapular spine rested along the posterior wall of the mold (Fig. 3d). The final skin mesh was then cut in half in the coronal plane using a slightly curved plane, which allowed for easier, more secured fitting in final assembly (Fig. 3b, c).

All 3D meshes were exported from Autodesk 3D Studio Max back into Materialise inPrint to ensure error-free 3D printability of the meshes. Each mesh was then individually exported as an STL file, ready for 3D printing.

3D printing and assembly of the shoulder phantom

3D printing was performed through a commercially available vendor, Materialise (Plymouth, MI, USA) utilizing three different technologies. Osseous structures were printed in gypsum (Fig. 4a, b), a calcium sulfate mineral ($CaSO_4{\cdot}2H_2O$), using binder jetting technology, where punctate liquid binding agents are deposited to join powder particles into solid objects. At the end of the printing process, "unglued" powder particle are "emptied" from the object. The capsule was 3D printed using rubber-like flexible TangoPlus material with Polyjet technology (Fig. 4c), where photopolymers are sprayed and cured with ultraviolet light during the printing process. Last, the skin mold was 3D-printed with polyamide (nylon) material (Fig. 5a–c) through selective laser sintering, where a high-powered laser solidifies and fuses powdered thermoplastics.

The printed humeral head and glenoid were placed into the capsule (Fig. 4d). The medial aspect of the capsule consisted of the glenoid surface and labrum, docked into the bony glenoid. The lateral aspect of the capsule was as an open socket; the humeral head telescoped into the open socket with a tight fit of the capsule onto the humeral head and tuberosity attachment sites. The capsule margins were glued using Smooth-On (Macungie, PA, USA) Sil-Poxy silicone rubber adhesive to the humeral head, creating a sealed cavity surrounding the joint and maintaining proper glenohumeral alignment.

The anchor points of the osseous structures inside the skin mold were covered by tape. The inside of the mold was sprayed with several coats of Smooth-On Ease Release 200 release agent, which facilitates release of the final silicone cast from the mold. The tape was removed after drying of the release agent. The 3D-printed bony structures and capsule were properly positioned inside the skin mold, and secured with Sil-Poxy silicone adhesive. The closed skin mold was secured with several rubber bands and small sand bags, and the two halves of the skin mold were joined and sealed with hot glue to prevent silicone leakage.

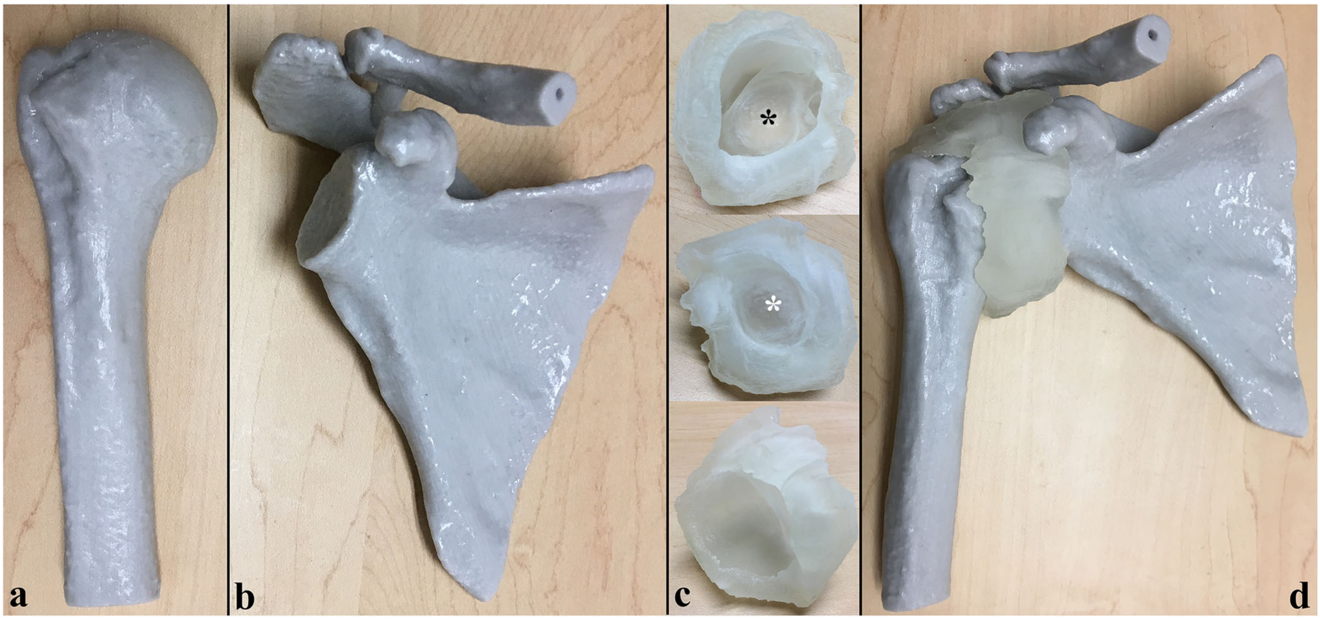

Fig. 4 The 3D printed components. **a**, **b** Rigid gypsum-based humerus, scapula, and clavicle, where the small strut stabilizing the clavicle is visible. **c** Rubber-like TangoPlus joint capsule, from lateral (*top*), medial (*middle*), and oblique (*bottom*) viewing angles. The glenoid cartilage (*asterisk*) can be seen with the edges representing the labrum. **d** Joint components assembled together. The glenoid docks into the medial aspect of the capsule and the humeral head telescopes into the open lateral aspect of the joint capsule; both were secured with glue

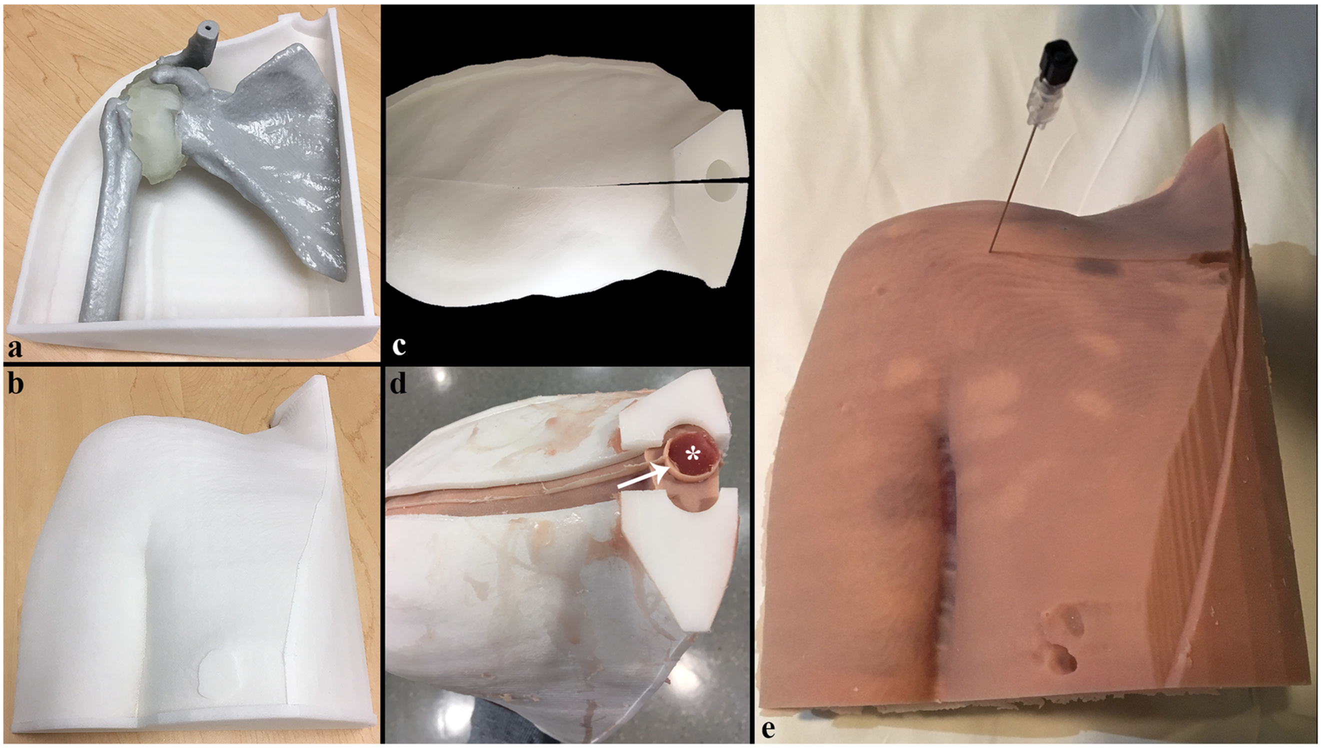

Fig. 5 All 3D printed components of the phantom before and after the molding process. **a** Humerus, scapula, and capsule placed in the posterior half of the skin mold. **b** Addition of the anterior half of the skin mold. **c** The two halves of the skin mold viewed from the top demonstrating the spout (for pouring of the silicone cast) and a slight gap between the two sides due to slight warping of the pieces, which was sealed with glue and tape before casting. **d** Opening the two skin mold pieces after casting, demonstrating the phantom's outer "skin" layer (*arrow*) and deeper "muscle" layer (*asterisk*). **e** Final appearance of the phantom with placement of a 22-gauge spinal needle for arthrography

The casting of the soft tissues in the mold was performed from the outside-in, using two-part platinum cure silicone that congeals after mixing the two parts in a 1:1 ratio. The superficial "skin" layer was created using strong dense silicone to maintain skin integrity for repeated use. Smooth-on Dragon Skin 10 silicone was pigmented and mixed with Smooth-on Silc Pig silicone colorant, and poured into the mold using a thin stream (to reduce trapping air bubbles in the silicone). The mold was rotated by hand to evenly coat the inside surface of the mold with a few millimeters of silicone. The mold was heated with a space heater to cure the silicone. The next layer of tissue, the subcutaneous fat, was cast using Smooth-On Ecoflex GEL, a softer, less dense silicone. This was also pigmented with Silc Pig, mixed, and poured into the mold. The mold was rotated and heated while it cured. The final deep thick layer of muscle tissue was created with an intermediate density Smooth-On Ecoflex 10 silicone. Given the large volume of silicone required for this step, the liquid silicone was initially placed into a vacuum-degassing chamber to remove air bubbles. The rest of the mold was completely filled with this de-gassed silicone, and heated for curing. The skin mold was removed (Fig. 5d), yielding the completed phantom (Fig. 5e).

Phantom shoulder arthrography & imaging

Fluoroscopic radiographs and CT of the shoulder phantom were obtained. Fluoroscopically guided shoulder arthrography was performed using anterior, posterior, and rotator interval approaches. CT arthrogram was also performed after intra-articular instillation of contrast medium.

Results

Fluoroscopic and CT imaging of the phantom

Fluoroscopic and CT images of the shoulder phantom are presented in Figs. 6 and 7. These images demonstrate the standard bony anatomy. Lucent air is present in the intra-articular space, which had to be created as an empty cavitary space, so that contrast medium could be instilled. The osseous structures were denser compared with an in-vivo shoulder, as confirmed by CT. The CT attenuation of the phantom's cortical bone, intramedullary bone, and soft tissues are compared with the in vivo shoulder, as summarized in Table 1 and demonstrated in Fig. 6a. Silicone rendering of the different soft-tissue layers could also be noted on the soft-tissue windows of the CT (Fig. 6b). The strong dense "skin" layer, the softer less dense "subcutaneous fat" layer, and intermediate density "muscular" layer of silicone had mean attenuations of 320 HU, 71 HU, and 133 HU respectively.

Phantom shoulder arthrography

Fluoroscopy-guided shoulder arthrography was successfully performed using rotator interval, anterior, and posterior approaches (Fig. 8a–c). These arthrographic techniques have been previously described [5–7]. An intra-articular osseous landing spot on the humeral head was targeted at the level of the rotator interval, mid-anterior and mid-posterior humeral head. Intra-articular access was confirmed with instillation of iodinated contrast medium, which was injected with little

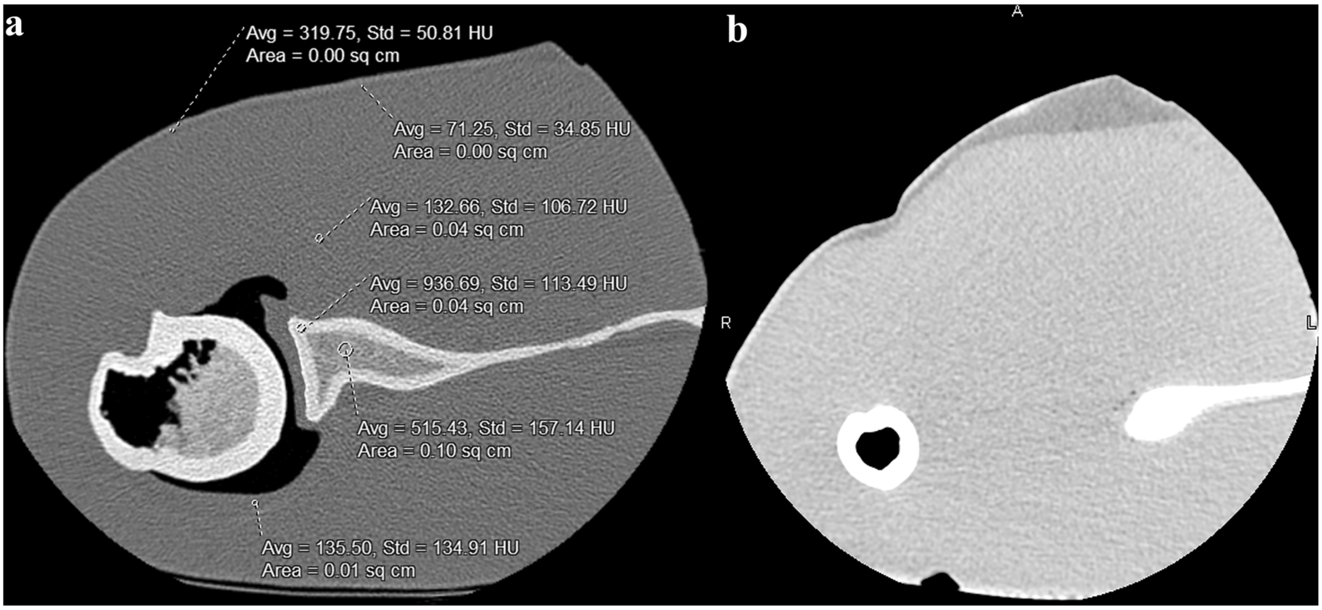

Fig. 6 Shoulder phantom CT. **a** Axial bone window demonstrating the CT attenuation in Hounsfield units of the various components. Note the corticomedullary differentiation in the osseous structures. Air tracked into the humerus after removal of unused gypsum during the printing process. **b** Axial soft-tissue window demonstrating dense skin, soft hypodense "subcutaneous fat," and intermediate density "muscle" layers

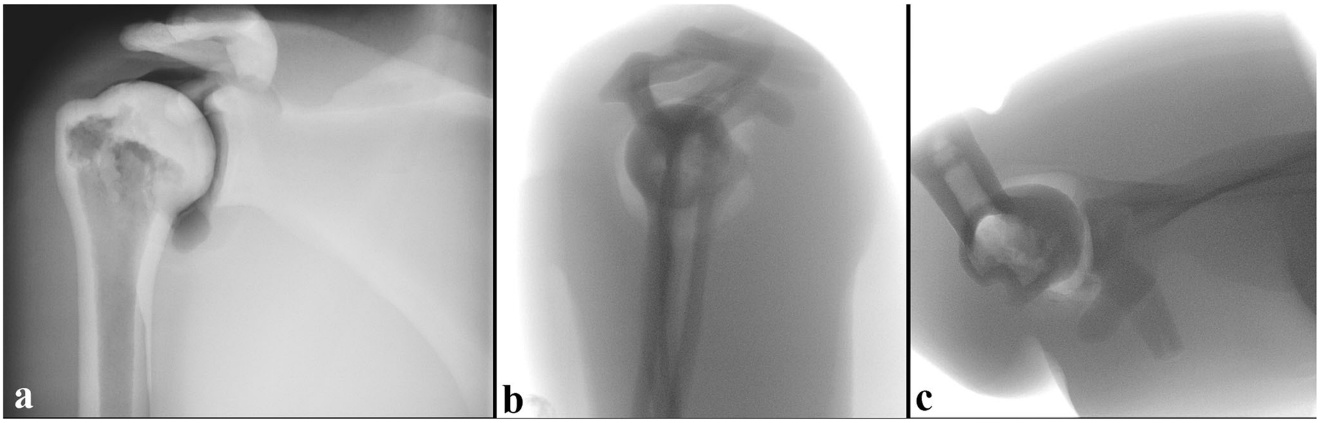

Fig. 7 Radiographic and fluoroscopic views of the shoulder phantom. **a** Grashey, **b** scapular Y-view, and **c** axillary views. Lucent air is visible in the glenohumeral joint and humerus. An air-filled cavitary space had to be rendered so that contrast medium could be instilled

resistance, flowing away from the injection site into the capacious joint space (Fig. 8d–f). Owing to the airtight contained cavitary nature of the intra-articular space, air had to be aspirated a few times from the glenohumeral joint as more contrast medium was injected with the same injection syringe, to completely fill the joint with contrast medium. Approximately 15 ml of contrast medium could be injected into the joint. The joint could be easily accessed via the rotator interval and posterior approach. The anterior approach was slightly more difficult because of the overhanging anterior labrum and middle glenohumeral ligament, requiring a slightly lateral to medial angled approach to avoid the labrum. CT arthrography images of the phantom were also obtained (Fig. 9), demonstrating a contrast medium-filled sealed intra-articular space and labrum along the glenoid.

At the end of arthrography, the intra-articular contrast medium was aspirated from the joint by positioning the phantom such that contrast medium was resting dependently along the intra-articular needle tip (i.e., the anterior approach injection required aspiration in the prone position). The intra-articular space was also irrigated a few times with saline to remove any residual contrast medium. All contrast medium was successfully removed from the joint in this manner, rendering the joint lucent and ready for repeat arthrography. When the needle was intentionally positioned in the extra-articular space, contrast medium could not be instilled into the dense surrounding silicone soft tissues, with significant pressure and resistance experienced at the syringe plunger.

Table 1 Comparison of the CT attenuation of the 3D printed phantom with an in vivo shoulder, both performed on the same scanner

Tissue	Mean attenuation ± SD (HU)	
	In vivo	Phantom
Cortical bone	548 ± 92	936 ± 113
Intramedullary bone	139 ± 108	515 ± 157
In vivo labrum and phantom TangoPlus capsule	65 ± 13	135 ± 134
Soft tissue (muscle)	65 ± 26	133 ± 107
Soft tissue (fat)	−98 ± 25	71 ± 35
Soft tissue (skin)	16 ± 10	320 ± 51

Mean values of three regions of interest placed in each of the described tissues for both an in vivo shoulder and the phantom

HU Hounsfield units, *SD* standard deviation

Discussion

Phantom arthrography

The phantom provided a reasonable model of the glenohumeral joint for the practice of arthrography. Fluoroscopic radiographs (Fig. 8) demonstrated adequate radiopaque bony structures of the shoulder, with visible bony landmarks, including the coracoid, greater and lesser tuberosities, and intertubercular sulcus. Air lucency is noted within the intra-articular space, which was constructed as an empty cavity for contrast medium instillation. The phantom's bones were denser on fluoroscopy and CT than in in vivo bone, although this did not have a negative impact on the visualization of bony landmarks. Radiographs and CT demonstrated successful 3D printing of osseous structures with corticomedullary differentiation. Dense cortical bone and less dense intra-medullary trabecular bone were able be printed for two reasons. First, during the initial software segmentation of the bone, pixels in the intramedullary cavity that did not meet the threshold attenuation of bone (pixels with fat, marrow or minimally calcified matrix) were rendered as an empty space in the mask layer (Fig. 1), and no gypsum deposition occurred in that voxel at 3D printing. These punctate empty spaces result in decreased intramedullary bony density. Second, gypsum-based 3D printing involves

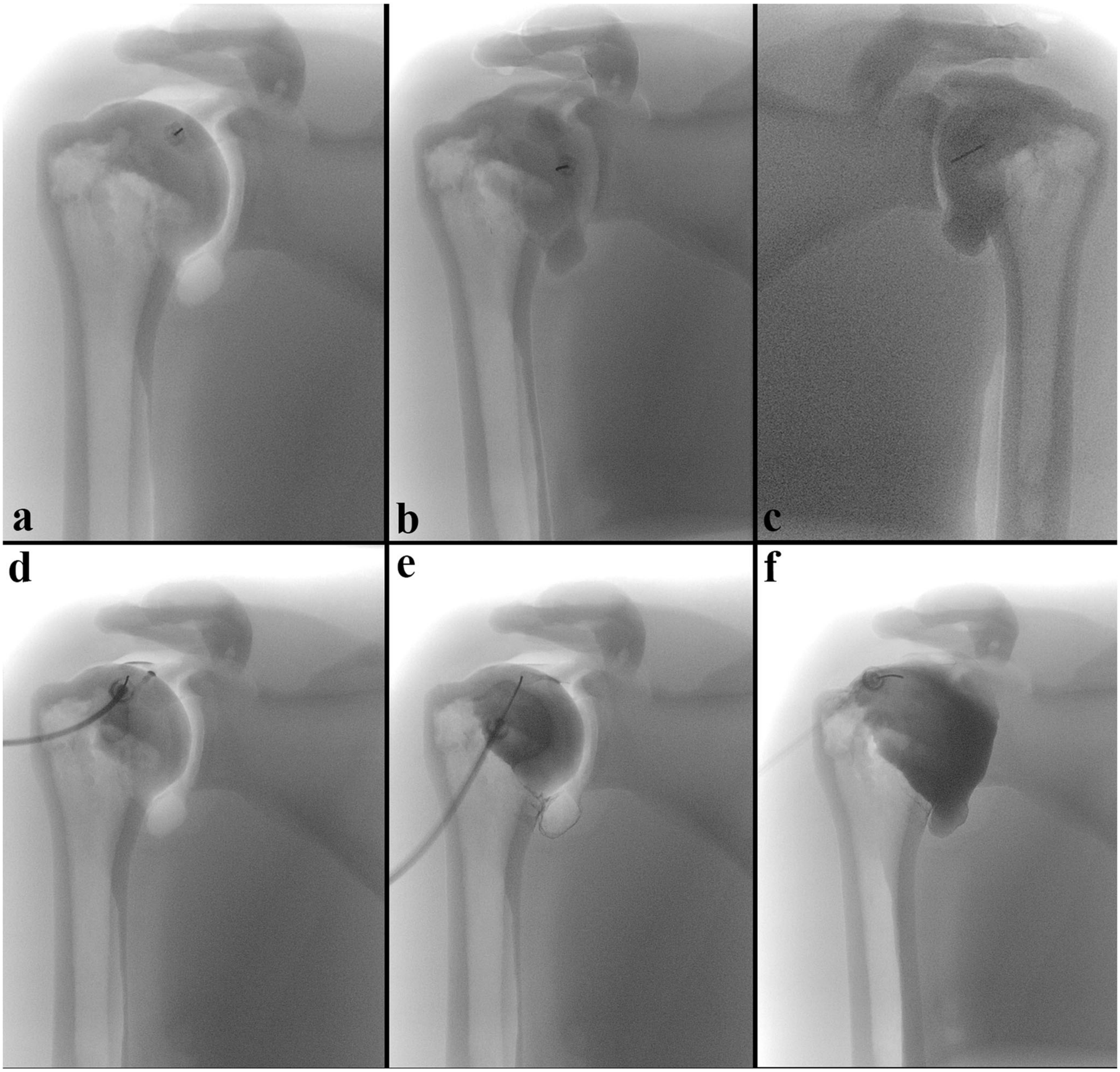

Fig. 8 Shoulder arthrography fluoroscopic images of the phantom using **a** a rotator interval approach, **b** an anterior approach, **c** a posterior approach. **d**–**f** Successive arthrography images from the rotator interval approach, demonstrating dispersion of the contrast medium from the needle tip into the joint, and eventual opacification of the joint with approximately 15 cm^3 of iodinated contrast medium

deposition of droplets of glue that adhere gypsum powder particles together during the printing process. At the end of printing, unglued gypsum particles are "emptied" from the structure as a fine powder. In the humerus, there was an opening in the intra-medullary cavity in the mid-diaphysis for removal of excess gypsum, with air subsequently tracking into this space, as seen on radiographs and CT (Figs. 6, 7). In the scapula, however, there was no opening for removal of unglued gypsum powder, which rendered the intramedullary cavity of the scapula slightly denser. The dense cortical bone provided a strong impenetrable bony surface "landing zone" for the arthrography needle.

The use of dense silicone for the skin surface and less dense layer of silicone for subcutaneous fat provided the phantom with a soft "life-like" feel. The deep intermediate density silicone for the muscular structures felt firm; differences in resistance could be felt as the needle passed from the "subcutaneous tissues" into the "muscle." During arthrography, the guidance of the needle mimicked in vivo dynamics. The

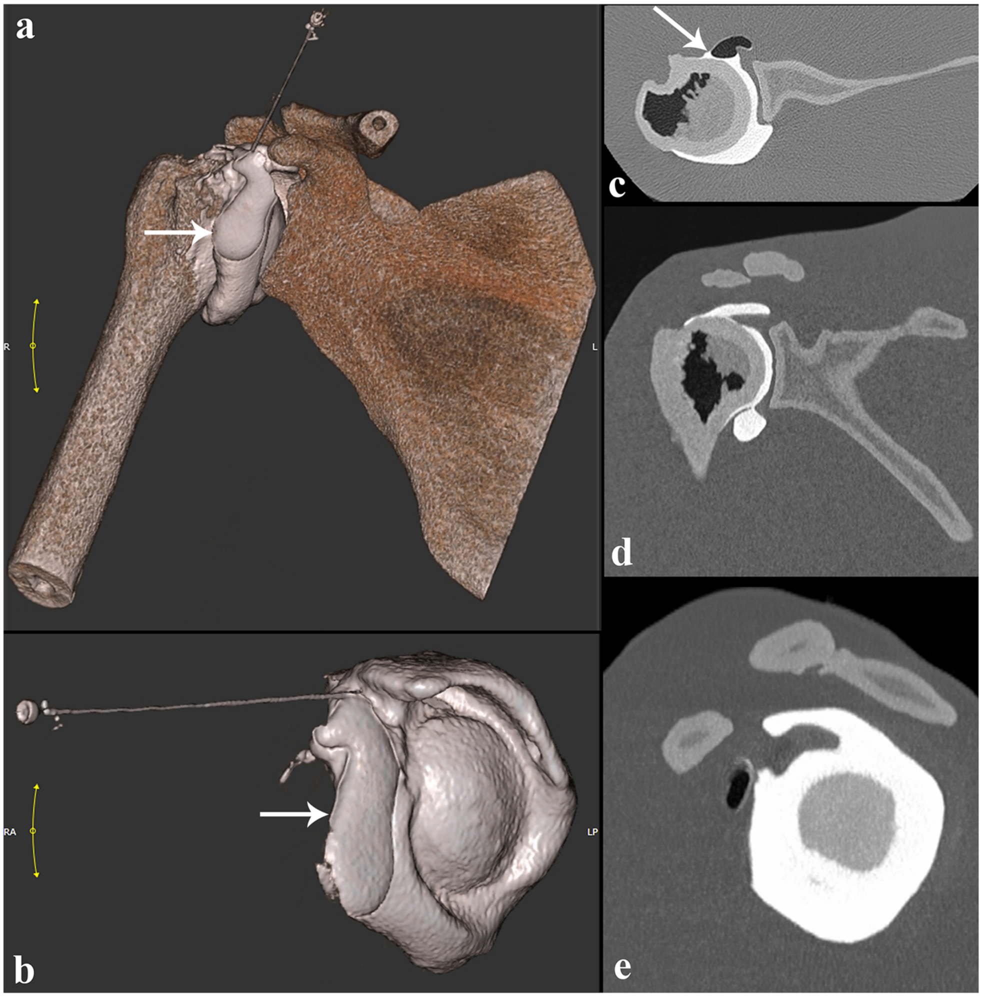

Fig. 9 CT arthrogram of the glenohumeral joint phantom after instillation of 15 cm^3 of iodinated contrast medium, which also demonstrates the air–contrast medium level (*arrows*), **a**, **b** 3D volume rendering, **c** axial, **d** coronal, and **e** sagittal planes

needle could be easily directed in the superficial tissues; it became more fixed in course the deeper it traveled, and required retraction for significant changes in direction. With the needle in the intra-capsular space, contrast medium was easily injected with minimal pressure. The contrast medium flowed away from the needle tip into the dependent portions of the joint, mimicking in vivo conditions. Approximately 15 ml of contrast medium could be instilled into this joint. At our institution, we instill 10–15 ml of contrast medium for shoulder arthrography based on the capaciousness of the joint. The CT scan used for this model was also selected for its capacious well-distended capsule to make joint access slightly easier for trainees.

We plan to use this model to teach shoulder arthrography to radiology residents in our department. Additional quality improvement metrics are required to assess its efficacy in building resident knowledge of and confidence in the procedure, decreasing fluoroscopy time, and minimizing patient discomfort. Dias et al. reported decreased fluoroscopy time, procedure time, and inappropriate needle positioning for radiology residents performing fluoroscopy-guided facet injections on phantoms [16]. Similarly, Faulkner et al. demonstrated decreased fluoroscopy time and increased operator confidence for residents who underwent lumbar puncture training on phantoms [22]. Increased operator confidence and reduced axial plane angular error have also been reported for CT-guided biopsies with phantom training [23].

Phantom construction

Several challenges were encountered in the 3D segmentation and printing of this phantom. A common problem encountered with threshold segmentation of anatomical structures is the exclusion of pertinent anatomy as absolute minimum and maximum threshold values have to be set. On in vivo CT images, the boundary between the high attenuation bone or contrast-enhanced intra-articular space and low attenuation surrounding soft tissues is a few pixels thick, with a gradual shift of attenuation across those pixels. Segmentation is binary in nature however; a pixel is segmented as part of the mask if it meets threshold cutoffs. This can lead to irregular and imperfect surface margins. As a result, a degree of manual segmentation is required for complex and intricate structures, which can be time-consuming. This was particularly applicable for the joint capsule.

The joint capsule segmentation and printing were also challenging in other ways. Initial consideration was given to 3D printing the entire capsule wall by itself as a collapsed cavity. Materialise inPrint has a "hollow" tool that can create a shell-like wall around the inside or outside of the margins of a segmentation mask, with a designated wall thickness. This was not feasible for a few reasons. The capsule had to be thin, soft, and penetrable by needle. The TangoPlus plastic material was ideal for this purpose; however, Polyjet printing of the capsule would not be feasible, as it would be extremely difficult if not impossible to completely "wash-out" the support material from such a narrow joint space. Furthermore, the narrowest gap in the in vivo glenohumeral joint was approximately 1 mm in width. However, direct 3D printing of the humeral and glenoid sides of the capsule wall (representing humeral head cartilage and the labrum respectively) with a thickness of at least 2 mm each and at least 2 mm of separation would create an unrealistic gap of at least 6 mm in vitro. It is noteworthy to mention that for the purposes of creating a radiographic phantom, Polyjet 3D printing of the osseous anatomy and the capsule simultaneously would not be possible with current technologies, as the bone could not be made radiodense and therefore would not be visible under fluoroscopy.

Direct 3D printing of the surrounding soft tissues was not feasible or practical for several reasons:

1. Fitting the osseous structures and capsule between into separately 3D printed solid surrounding soft tissues would be very difficult, time-consuming, and logistically nearly impossible.
2. 3D printing such a high volume of material would be very costly.
3. There are a limited number of 3D printable soft materials that can be easily penetrated by a needle.

As a result, a polyamide skin mold and the silicone casting technique were implemented. The skin mold was printed in polyamide, which has a grainy porous surface, and rendered the final casted soft tissues with a slightly nodular surface. Although a resin mold could have been printed for its smoother surface, allowing easier separation from the silicone, it is significantly more expensive and has a higher likelihood for warping compared with polyamide. Even the printed polyamide mold developed slight warping, causing a small gap between the two halves, as noted in Fig. 5c. This gap was sealed with glue before the silicone molding process. Silicone was used because it is widely available, relatively inexpensive, durable, easy to work with, can have variable density, and has been used extensively in anatomical models. Softer, less dense silicone was used for the subcutaneous fat, intermediate density silicone was used for deep muscular structures, and the strongest silicone was used for the thin skin layer; this difference in density was palpable as the needle was advanced during arthrography.

The following shows the cost of each 3D printed part: humerus \$245, scapula \$265, capsule \$225, skin mold (anterior half) \$355, skin mold (posterior half) \$385, totaling to \$1,475. This included an approximately 20% mark-up because of the medical grade nature of the order. If ordered through the public Materialise website, the cost would approximately be \$1,180. These parts were printed by the vendor within 2 weeks. The cost of silicone, glue, and spray was approximately \$145. The total time needed for segmentation, 3D printing, and assembly was approximately 6 weeks.

Limitations and future directions

There are a few limitations with this phantom. The model had to be constructed in a neutral position as the segmentation masks were developed based on a CTA with the patient in neutral position. The silicone soft tissues of the shoulder lock the glenohumeral joint in this position. Although shoulder arthrography via an anterior and rotator interval approach is typically performed with the humerus in external rotation, arthrography was successful with the phantom in this position. The phantom's air-containing lucent intra-capsular space was fluoroscopically visible and provided a slightly larger intra-articular landing space for the needle compared with a collapsed joint capsule in vivo. For training purposes, trainees were instructed to use bony landmarks to guide needle placement and inject only when the needle had landed on their bony target. Future iterations of the capsule could be made with an elastic waterproof fabric that could collapse and expand to more closely mimic the in vivo capsule and decrease visible air lucency, although adhesion of such a fabric to the gypsum bone at anatomically accurate insertion points will be difficult. The phantom was created using the CT arthrography image data from a young thin patient with normal anatomy; patients typically seen for arthrography deviate from this paradigm. Increased body mass index has been shown to correlate with increased fluoroscopy time with lumbar punctures [24]. Image data from larger patients with degenerative changes could be used for other phantom iterations.

Given the cost of this model, it is notable that the model has exhibited durability for several months of use with no visible signs of wear or tear including at the needle entry site. Future phantoms could also be printed with less calcium-rich gypsum (which is currently not available) to more closely approximate bony density, or by adjusting the segmentation thresholds to "extract" less bone into the mask and therefore print less bone.

The joint capsule could alternatively be created as a soft silicone cast of the intra-articular space, which would better allow for failed extracapsular injection. This, however, could affect the long-term reusability of the phantom. Fused deposition modeling (FDM), which prints extruded melted plastic filaments, could print a 3D mesh of the intra-articular space made of polyvinyl alcohol (PVA); silicone could be cast over this mold, and the PVA could then be dissolved by water through a small opening [25]. The silicone soft tissues could also be improved upon. Although silicone is soft and suitable for soft tissues that undergo repeated needle punctures, contributing to the durability of our phantom, it is not the most life-like material. It is difficult for silicone, or any other single homogeneous material, to render the tactile “feel” of real soft tissue, which consists of multiple different tissues and densities (dermis collagen scaffolds, fat lobules, muscle fibers, etc.). Alternatives to silicone, including hydrogel (gelatin/agar), polyvinyl alcohol cryogel, and gellan gum, have also been described [26–28]; although these have more life-like haptic “feel,” they are less durable and require much more preparation. In the future, multi-material 3D printers may be able to print such soft material directly onto different dense material. Given the silicone soft tissues in our model, the joint cannot be imaged with ultrasound. Polyvinyl alcohol cryogel or ballistic high concentration gelatin could be used for the soft tissues in future models to create dual modality phantoms that are also suitable for ultrasound-guided arthrography training as well [29].

Acknowledgements The authors would like to thank Maureen Schickel from Materialise for offering her technical expertise.

Compliance with ethical standards

Conflicts of interest The authors declare that they have no conflicts of interest.

References

1. Lomasney LM, Choi H, Jayanthi N. Magnetic resonance arthrography of the upper extremity. Radiol Clin N Am. 2013;51(2):227–37.
2. Malfair D. Therapeutic and diagnostic joint injections. Radiol Clin N Am. 2008;46(3):439–53.
3. Magee T. 3-T MRI of the shoulder: is MR arthrography necessary? AJR Am J Roentgenol. 2009;192(1):86–92.
4. Probyn LJ, White LM, Salonen DC, Tomlinson G, Boynton EL. Recurrent symptoms after shoulder instability repair: direct MR arthrographic assessment–correlation with second-look surgical evaluation. Radiology. 2007;245(3):814–23.
5. Jacobson JA, Lin J, Jamadar DA, Hayes CW. Aids to successful shoulder arthrography performed with a fluoroscopically guided anterior approach. Radiographics. 2003;379;23(2):373–8; discussion 379.
6. Farmer KD, Hughes PM. MR arthrography of the shoulder: fluoroscopically guided technique using a posterior approach. AJR Am J Roentgenol. 2002;178(2):433–4.
7. Depelteau H, Bureau NJ, Cardinal E, Aubin B, Brassard P. Arthrography of the shoulder: a simple fluoroscopically guided approach for targeting the rotator cuff interval. AJR Am J Roentgenol. 2004;182(2):329–32.
8. Friedman T, Michalski M, Goodman TR, Brown JE. 3D printing from diagnostic images: a radiologist's primer with an emphasis on musculoskeletal imaging-putting the 3D printing of pathology into the hands of every physician. Skeletal Radiol. 2016;45(3):307–21.
9. Auricchio F, Marconi S. 3D printing: clinical applications in orthopaedics and traumatology. EFORT Open Rev. 2016;1(5):121–7.
10. Numminen K, Sipila O, Makisalo H. Preoperative hepatic 3D models: virtual liver resection using three-dimensional imaging technique. Eur J Radiol. 2005;56(2):179–84.
11. Esses SJ, Berman P, Bloom AI, Sosna J. Clinical applications of physical 3D models derived from MDCT data and created by rapid prototyping. AJR Am J Roentgenol. 2011;196(6):W683–8.
12. Vukicevic M, Mosadegh B, Min JK, Little SH. Cardiac 3D printing and its future directions. J Am Coll Cardiol Imaging. 2017;10(2):171–84.
13. Javan R, Herrin D, Tangestanipoor A. Understanding spatially complex segmental and branch anatomy using 3D printing: liver, lung, prostate, coronary arteries, and circle of Willis. Acad Radiol. 2016;23(9):1183–9.
14. Tai BL, Rooney D, Stephenson F, Liao P, Sagher O, Shih AJ, et al. Development of a 3D-printed external ventricular drain placement simulator: technical note. J Neurosurg. 2015;123(4):1070–6.
15. O'Reilly MK, Reese S, Herlihy T, Geoghegan T, Cantwell CP, Feeney RNM, et al. Fabrication and assessment of 3D printed anatomical models of the lower limb for anatomical teaching and femoral vessel access training in medicine. Anat Sci Educ. 2016;9(1):71–9.
16. Dias TR, Alves Junior JDC, Abdala N. Learning curve of radiology residents during training in fluoroscopy-guided facet joint injections. Radiol Bras. 2017;50(3):162–9.
17. Ali S, Qandeel M, Ramakrishna R, Yang CW. Virtual simulation in enhancing procedural training for fluoroscopy-guided lumbar puncture: a pilot study. Acad Radiol. 2018;25(2):235–9.
18. Javan R, Bansal M, Tangestanipoor A. A prototype hybrid gypsum-based 3-dimensional printed training model for computed tomography-guided spinal pain management. J Comput Assist Tomogr. 2016;40(4):626–31.
19. Pham DL, Xu C, Prince JL. Current methods in medical image segmentation. Annu Rev Biomed Eng. 2000;2:315–37.
20. Mitsouras D, Liacouras P, Imanzadeh A, Giannopoulos AA, Cai T, Kumamaru KK, et al. Medical 3D printing for the radiologist. Radiographics. 2015;35(7):1965–88.
21. Shirazi SFS, Gharehkhani S, Mehrali M, Yarmand H, Metselaar HSC, Kadri NA, et al. A review on powder-based additive manufacturing for tissue engineering: selective laser sintering and inkjet 3D printing. Sci Technol Adv Mater. 2015;16(3):033502. https://doi.org/10.1088/1468-6996/16/3/033502.
22. Faulkner AR, Bourgeois AC, Bradley YC, Pasciak AS. A robust and inexpensive phantom for fluoroscopically guided lumbar puncture training. Simul Healthc. 2015;10(1):54–8.
23. Dimmick S, Jones M, Challen J, Iedema J, Wattuhewa U, Coucher J. CT-guided procedures: evaluation of a phantom system to teach accurate needle placement. Clin Radiol. 2007;62(2):166–71.
24. Boddu SR, Corey A, Peterson R, Saindane AM, Hudgins PA, Chen Z, et al. Fluoroscopic-guided lumbar puncture: fluoroscopic time and implications of body mass index—a baseline study. AJNR Am J Neuroradiol. 2014;35(8):1475–80.
25. Liu Y, Gao Q, Du S, Chen Z, Fu J, Chen B, et al. Fabrication of cerebral aneurysm simulator with a desktop 3D printer. Sci Rep. 2017;7:44301.

26. Chen RK, Shih AJ. Multi-modality gellan gum-based tissue-mimicking phantom with targeted mechanical, electrical, and thermal properties. Phys Med Biol. 2013;58(16):5511–25.
27. Ryan JR, Chen T, Nakaji P, Frakes DH, Gonzalez LF. Ventriculostomy simulation using patient-specific ventricular anatomy, 3D printing, and hydrogel casting. World Neurosurg. 2015;84(5):1333–9.
28. Morais P, Tavares JMRS, Queiros S, Veloso F, D'hooge J, Vilaca JL. Development of a patient-specific atrial phantom model for planning and training of inter-atrial interventions. Med Phys. 2017;44(11):5638–49.
29. Javan R, Cho AL. An assembled prototype multimaterial three-dimensional-printed model of the neck for computed tomography- and ultrasound-guided interventional procedures. J Comput Assist Tomogr. 2017;41(6):941–8.